Interception in Three Dimensions: An Energy Formulation

N. Rajan*
Stanford University, Stanford, California
and
M.D. Ardema†
NASA Ames Research Center, Moffett Field, California

The problem of minimum-time interception of a target flying in three-dimensional space is analyzed with the interceptor aircraft modeled through the energy-state approximation. A coordinate transformation that uncouples the interceptor's extremals from the target motion in an open-loop sense is introduced, and the necessary conditions for optimality and the optimal controls are derived. Special attention is devoted to the determination of extremal values of the speed, which appears as a control variable in the energy-state model. Example extremals for a high-performance aircraft are computed. The extremal paths typically consist of segments on the corner-velocity locus and on the maximum speed boundary, and exhibit discontinuities in speed.

Nomenclature

$a(h)$ = speed of sound
$A(V,E)$ = $T_M(M,h)/W$
$B(V,E)$ = $(D_o + D_{Lo})/W$
$C(V,E)$ = $D_{Lo}\tan^2\theta_M/W$
$C_{Do}(M)$ = base drag coefficient
$C_L(M,\alpha)$ = lift coefficient
C_{L_α} = lift coefficient slope with respect to angle of attack
$D(h,V,\alpha)$ = drag
$D_o(M,h)$ = base drag, qSC_{Do}
$D_{Lo}(M,h)$ = lift-induced drag at zero bank, $qSC_L\eta\alpha$
E = specific energy
$f(V,E)$ = maximum instantaneous turn rate (MITR), $g\tan\theta_M(M,h)/V$
g = acceleration due to gravity
h = altitude
$h_m(E)$ = lower limit on altitude
$h_M(E)$ = upper limit on altitude
H = Hamiltonian
$\bar{H}$ = Hamiltonian normalized by division with $2\nu R$
$L(h,V,\alpha)$ = lift, qSC_L
LOS = horizontal line of sight
m = aircraft mass
M = Mach number, V/a
MITR = maximum instantaneous turn rate
n = maximum load factor
p_E = energy adjoint
q = dynamic pressure, $(\frac{1}{2})\rho V^2$
r = horizontal line-of-sight length
R = capture radius
S = wing reference area
t = time
$T(\pi,h,V)$ = thrust
V = speed
$V_c(E)$ = corner velocity
$V_m(E)$ = lower speed limit due to loft ceiling
$V_M(E)$ = upper speed limit due to terrain, dynamic pressure, or maximum velocity placard limit
$V_p(E)$ = maximum velocity placard limit
W = aircraft weight
(x,y) = horizontal position coordinates
α = angle of attack
α_M = stall angle of attack
γ = flightpath angle
θ = bank angle
$\theta_M(M,h)$ = upper limit on bank angle due to maximum load factor or stall-limit
λ = adjoint variable
μ = Kuhn-Tucker multiplier
$\bar{\mu}$ = normalized multiplier
ν = multiplier
π = throttle setting
$\rho(h)$ = atmospheric density
τ = retrograde time, $t_f - t$
χ = heading
ω = $\tan\theta/\tan\theta_M$
$\eta(M)$ = efficiency factor

Subscripts

I = interceptor
m = minimum
M = maximum
p = placard
T = target
f = quantities at the final instant
x,y,χ,E = corresponding to the specified state variable

Introduction

TRAJECTORY optimization for high-performance aircraft remains a difficult problem despite recent advances in analytical and computational techniques. The governing differential equations are highly coupled, nonlinear, and of high order. Many of the quasisteady approximations made in the analysis of transport aircraft and other low-performance vehicles are not valid for the highly dynamic maneuvers typical of high-performance military aircraft. Nevertheless, there has been recent progress in solving an important trajectory-optimization problem for high-performance aircraft, namely the minimum-time interception of a target.

Presented as Paper 83-2121 at the AIAA Atmospheric Flight Mechanics Conference, Gatlinburg, Tenn., Aug. 15-17, 1983; received Aug. 30, 1983; revision received Jan. 3, 1984. This paper is declared a work of the U.S. Government and therefore is in the public domain.

*Research Associate. Member AIAA.
†Research Scientist. Associate Fellow AIAA.

Direct and indirect numerical methods of solving the interception problem have been reported.[1,2] In Ref. 1, optimal evasion against a pursuer flying pure pursuit is determined by parameter-optimization methods. In Ref. 2, extremal controls for pursuit-evasion in a horizontal plane are computed using a differential dynamic programming algorithm. Both these approaches generate open-loop solutions from given initial conditions, assuming that the given initial state is within the state-space capture region. Realistic point-mass aircraft models were employed in both analyses.

Another approach to the problem is based on singular-perturbation theory, which relies on inherent time-scale separations to uncouple the system of differential equations into low-order systems. Much of this work is reviewed in Ref. 3. Two notable examples of this approach applied to target interception are reported in Refs. 4 and 5, in both of which extremal controls in feedback form are derived. These feedback control laws have potential for on-board, automatic, flightpath management, although their validity is largely untested.

In Refs. 6-11, open-loop and feedback controls and corresponding extremals have been generated for both target interception and pursuit-evasion in a horizontal plane. In this paper we consider target interception in three dimensions, using the energy-state dynamic model. Realistic aerodynamic and propulsive force models and realistic state and control constraints for high-performance aircraft are used. The resulting optimal control problem has the same dimension as the horizontal-plane problem. Just as in the horizontal-plane case, a unique reference frame is found which, in a certain sense, decouples the open-loop extremals of the interceptor from the target motion.

Three-Dimensional Energy-State Model

The most general system of differential equations commonly employed in aircraft trajectory analysis is the following sixth-order system:

$$\left.\begin{aligned}
\dot{x} &= V\cos\gamma\cos\chi \\
\dot{y} &= V\cos\gamma\sin\chi \\
\dot{h} &= = V\sin\gamma \\
\dot{V} &= g(T-D)/W - g\sin\gamma \\
\dot{\chi} &= gL\sin\theta/WV\cos\gamma \\
\dot{\gamma} &= gL\cos\theta/WV - g\cos\gamma/V
\end{aligned}\right\} \tag{1}$$

where $T=T(\pi,h,V)$, $D=D(h,V,\alpha)$, and $L=L(h,V,\alpha)$. These equations embody the assumptions of a constant-weight, point-mass (particle) aircraft with thrust aligned along the velocity vector; a flat nonrotating Earth; symmetric flight; and constant gravitational attraction. The control variables in these equations are α, θ, and π.

Because of the relatively high-order and highly nonlinear nature of Eqs. (1), there has been little practical application of them. Instead, attention has focused on reduced-order systems.[12] These reduced-order analyses are based on either restricting the motion to a special case, such as flight in either a horizontal or a vertical plane, on ad-hoc time-scale separations, or both. Reference 3 describes many past analyses based on reduced-order systems.

For the restricted case of flight in a vertical plane, the introduction of the specific energy as a state variable has proved to be advantageous, especially when further order reduction by time-scale separation is employed. This transformation is also possible and desirable in the three-dimensional case.[12] The specific energy of the aircraft, or energy per unit weight, is defined as

$$E = V^2/2g + h \tag{2}$$

Differentiating and using Eq. (1) gives

$$\dot{E} = V(T-D)/W \tag{3}$$

Substitution of E for V in the equations of motion then gives

$$\dot{x} = V\cos\gamma\cos\chi \tag{4a}$$

$$\dot{y} = V\cos\gamma\sin\chi \tag{4b}$$

$$\dot{h} = V\sin\gamma \tag{4c}$$

$$\dot{E} = V(T-D)/W \tag{4d}$$

$$\dot{\chi} = gL\sin\theta/WV\cos\gamma \tag{4e}$$

$$\dot{\gamma} = \mathrm{gL}\cos\theta/WV - g\cos\gamma/V \tag{4f}$$

where from Eq. (2),

$$V(E,h) = [2g(E-h)]^{1/2} \tag{5}$$

We now assume that there is a time-scale separation between (x,y,E,χ) and (h,γ) such that (h,γ) vary on a much faster time-scale than do the other variables and, therefore, to a first approximation, their dynamics can be neglected. Consistent with singular-perturbation theory (cf. Ref. 13), we then set $\dot{h}=0$ and $\dot{\gamma}=0$ in Eqs. (4c) and (4f) to obtain the algebraic constraints,

$$\gamma = 0 \tag{6a}$$

$$L\cos\theta = W \tag{6b}$$

and the remaining state equations become the reduced-order system,

$$\left.\begin{aligned}
\dot{x} &= V\cos\chi \\
\dot{y} &= V\sin\chi \\
\dot{E} &= V(T-D)/W \\
\dot{\chi} &= gL\sin\theta/WV
\end{aligned}\right\} \tag{7}$$

This fourth-order system is the three-dimensional energy-state model[12]; the control variables are π, L (or θ), and V (or h).

It is assumed that the aerodynamic and propulsive forces have the form

$$\left.\begin{aligned}
T(\pi,h,V) &= \pi T_M(h,M) \\
D(h,V,\alpha) &= [C_{D_o}(M) + \eta(M) C_{L_\alpha}(M)\alpha^2]\,\tfrac{1}{2}\rho(h)V^2S \\
L(h,V,\alpha) &= \tfrac{1}{2}\rho(h)V^2SC_{L_\alpha}(M)\alpha
\end{aligned}\right\} \tag{8}$$

and that the constraints on the state and control variables are specified by

$$0 \le \pi \le 1 \text{ (throttle)} \tag{9a}$$

$$L \le \min[C_{L_\alpha}(M)\alpha_M \tfrac{1}{2}\rho(h)V^2S, nW] \text{ (lift)} \tag{9b}$$

$$h \ge 0 \text{ (terrain)} \tag{9c}$$

$$C_{L_\alpha}(M)\alpha_M \tfrac{1}{2}\rho(h)V^2S \ge W \text{ (loft ceiling)} \tag{9d}$$

$$V \le V_p(E) \text{ (placard)} \tag{9e}$$

Next, we make a change of control variable.[6-9] Let

$$\omega = \tan\theta/\tan\theta_M \tag{10}$$

where from Eqs. (6b) and (9b)

$$\theta_M(M,h) = \sec^{-1}\left\{\min\left[\frac{C_{L_\alpha}(M)\alpha_M\rho(h)V^2S}{2W}, n\right]\right\} \tag{11}$$

Substituting θ for L from Eq. (6b) and ω for θ from Eq. (10) in Eqs. (7), the latter are modified as follows:

$$\left.\begin{aligned}\dot{x} &= V\cos\chi\\ \dot{y} &= V\sin\chi\\ \dot{E} &= V[A(V,E)\pi - B(V,E) - C(V,E)\omega^2]\\ \dot{\chi} &= \omega f(V,E)\end{aligned}\right\} \tag{12}$$

where

$$\left.\begin{aligned}A(V,E) &= T_M(h,M)/W\\ B(V,E) &= [D_o(M,h) + D_{Lo}(M,h)]/W\\ C(V,E) &= D_{Lo}(M,h)V^2f^2(V,E)/g^2W\end{aligned}\right\} \tag{13}$$

Here, $D_o(M,h)$ and $D_{Lo}(M,h)$ are the zero-lift drag and the drag resulting from lift at zero bank, respectively. From Eq. (2), h is now regarded as a function of V and E

$$h(V,E) = E - V^2/2g \tag{14}$$

The function $f(V,E)$ in Eq. (12) is the maximum instantaneous turn rate (MITR). The control variables are now taken as π, ω, and V; since V is a control variable, instantaneous changes in V (and, hence, also in h) are now possible. This is the major unrealistic feature of the energy-state model. The constraint Eqs. (9) are rewritten as

$$0 \le \pi \le 1 \tag{15a}$$

$$-1 \le \omega \le 1 \tag{15b}$$

$$V_m(E) \le V \le V_M(E) \tag{15c}$$

where $V_m(E)$ denotes the loft ceiling and $V_M(E)$ is the maximum speed, given by the terrain constraint at low speeds and the placard limit at high speeds.

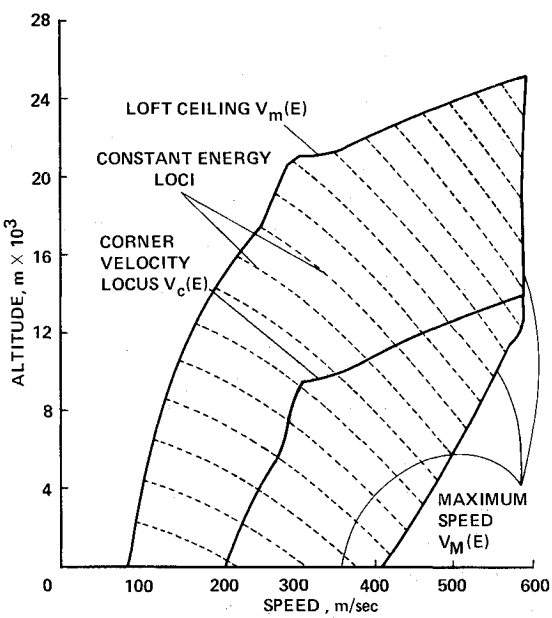

Fig. 1 Aircraft flight envelope (F-4C aircraft model).

The corner velocity locus $V_c(E)$ will play an important part in the analysis that follows; it is defined as the velocity for which the two lift constraints in Eq. (9b) are equal:

$$C_{L_\alpha}(E,V_c)\alpha_M\rho(E,V_c)V_c^2S/2 = nW \tag{16}$$

The corner-velocity locus is the locus of maximum MITR.[3] Figure 1 shows the corner-velocity locus as well as the flight envelope as defined by Eq. (15c) for a typical high-performance aircraft.

Minimum-Time Interception

In the minimum-time-interception problem, one aircraft, designated the interceptor, wishes to capture another aircraft, designated the target, in minimum time. It is assumed that the motion of the target is specified by its positional coordinates $[x_T(t), y_T(t), h_T(t)]$ in some fixed reference frame and that these functions, and, hence, all other target variables, are known to the interceptor. In the same coordinates, the interceptor's motion is governed by Eq. (12) subject to Eq. (15). Capture is defined to occur when 1) the projection of the line-of-sight in the horizontal plane (LOS) is a specified value, 2) the LOS is decreasing, and 3) the interceptor can select his altitude to be within a specific vertical distance δh of the target's altitude; that is, when all three of the following criteria are satisfied:

$$\left.\begin{aligned}&r_f = R\\ &\dot{r}_f \le 0 \text{ for some } h_f \in [h_{Tf} - \delta h, h_{Tf} + \delta h]\\ &h_{Tf} \in [h_{mf} - \delta h, h_{Mf} + \delta h]\end{aligned}\right\} \tag{17}$$

These relations reflect the fact that in general, the interceptor's altitude (and velocity) will jump discontinuously at termination. The vertical-plane conditions of Eq. (17) are illustrated in Fig. 2. The horizontal LOS distance is given by

$$r^2(t) = [x(t) - x_T(t)]^2 + [y(t) - y_T(t)]^2 \tag{18}$$

The reference frame chosen for the encounter has its origin at the interceptor's position at capture (assuming capture to occur) with the x-axis along the terminal LOS. As in the planar case,[6-11] this reference frame has the great advantage that the terminal transversality conditions for the two aircraft uncouple (as will be shown subsequently) but has the disadvantage that the reference frame varies from interception to interception. Using Eqs. (7), (14), (15), and (18), in this reference frame Eqs. (17) may be written as

$$(x_f - x_{Tf})^2 + (y_f - y_{Tf})^2 = R^2 \tag{19a}$$

$$V_f\cos\chi_f - V_{Tf}\cos\chi_{Tf}\cos\gamma_{Tf} \ge 0 \quad \text{for some}$$

$$V_f \in [\sqrt{2g(E_f - h_{Tf} - \delta h)},\ \sqrt{2g(E_f - h_{Tf} + \delta h)}] \tag{19b}$$

$$h_{Tf} \in \left[E_f - \frac{1}{2g}V_M^2(E_f) - \delta h,\ E_f - \frac{1}{2g}V_m^2(E_f) + \delta h\right] \tag{19c}$$

Note that only the x-component of the target's terminal velocity influences $\dot{r}_f$. A typical interception is depicted in Fig. 3, in which it is assumed that $\delta h = 0$.

The performance index for minimum time, augmented by the terminal constraint (19a), is

$$J = \nu[(x_f - x_{Tf})^2 + (y_f - y_{Tf})^2 - R^2] + \int_0^{t_f} dt \tag{20}$$

The presence of the target motion in J makes the system nonautonomous. From Eqs. (12) and (20), the variational

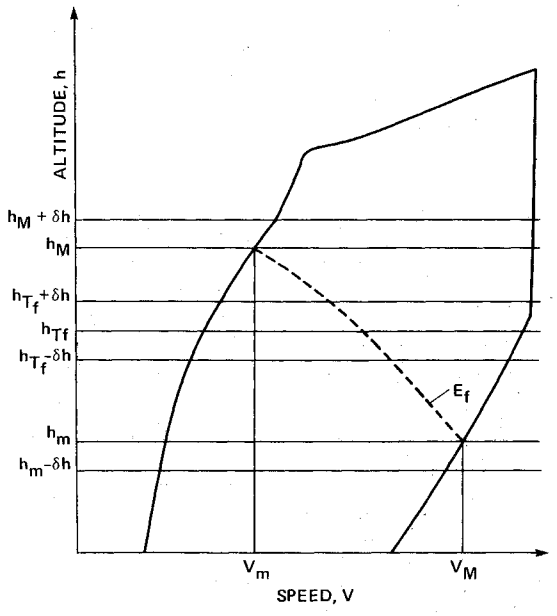

Fig. 2 Conditions at capture.

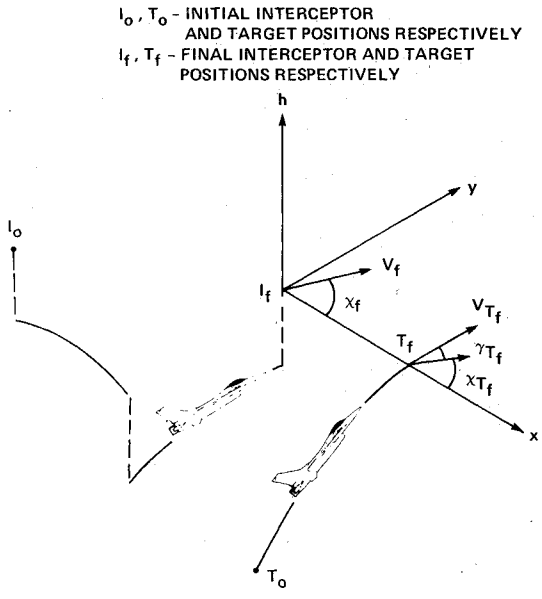

Fig. 3 Choice of coordinate axes.

Hamiltonian for this problem is

$$H = 1 + \lambda_x V\cos\chi + \lambda_y V\sin\chi + \lambda_E V(A\pi - B - C\omega^2) + \lambda_\chi \omega f + \mu(V - V_m)(V - V_M) \tag{21}$$

where the multiplier μ accounts for the constraints on the speed, Eq. (15), and satisfies the condition

$$\mu \begin{cases} > 0, & \text{if } V = V_m \text{ or } V_M \\ = 0, & \text{if } V_m < V < V_M \end{cases} \tag{22}$$

The maximum principle[14,15] will now be applied to obtain the necessary conditions for optimal interception. The adjoint equations are

$$\dot{\lambda}_x = 0 \tag{23a}$$

$$\dot{\lambda}_y = 0 \tag{23b}$$

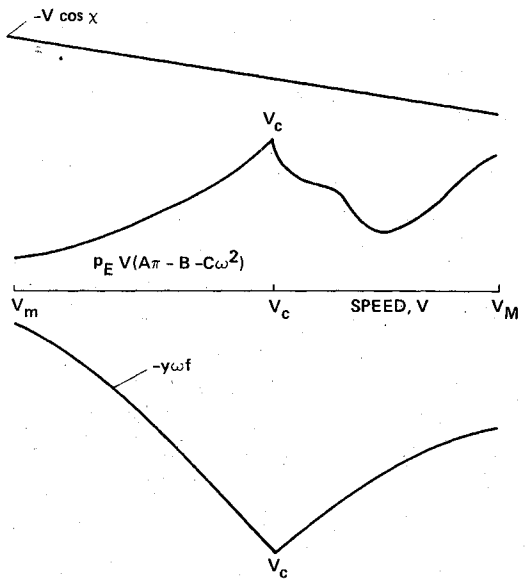

Fig. 4 Sketch of the three individual terms in the Hamiltonian.

$$\dot{\lambda}_\chi = \lambda_x V\sin\chi - \lambda_y V\cos\chi \tag{23c}$$

$$\dot{\lambda}_E = -\lambda_\chi \omega \frac{\partial f}{\partial E} - \lambda_E V\left(\frac{\partial A}{\partial E}\pi - \frac{\partial B}{\partial E} - \frac{\partial C}{\partial E}\omega^2\right) + \mu\left[(V - V_M)\frac{dV_m}{dE} + (V - V_m)\frac{dV_M}{dE}\right] \tag{23d}$$

Equations (23a)-(23c) may be integrated to give

$$\left.\begin{aligned} \lambda_x &= C_1 \\ \lambda_y &= C_2 \\ \lambda_\chi &= C_1 y - C_2 x + C_3 \end{aligned}\right\} \tag{24}$$

where the C_i are constants. The boundary conditions are

$$x_f = y_f = 0 \tag{25}$$

and the transversality conditions are (note that $x_{Tf} = R$ and $y_{Tf} = 0$)

$$\left.\begin{aligned} \lambda_{\chi f} = \lambda_{Ef} = \lambda_{yf} &= 0 \\ \lambda_{xf} &= -2\nu R \end{aligned}\right\} \tag{26}$$

Using Eqs. (25) and (26) in Eqs. (24), we have

$$\left.\begin{aligned} \lambda_x &= -2\nu R \\ \lambda_y &= 0 \\ \lambda_\chi &= -2\nu R y \end{aligned}\right\} \tag{27}$$

The additional terminal condition gives

$$\nu = [2R(V_f\cos\chi_f - V_{Tf}\cos\chi_{Tf}\cos\gamma_{Tf})]^{-1} > 0 \tag{28}$$

where ν is positive because the target's x-component of velocity must be less than the interceptor's at capture.

The optimal controls are given by

$$\pi, \omega, V = \arg\left[\min_{(\pi,\omega,V)} H\right] \tag{29}$$

The minimum value of H is a constant which can be evaluated at termination; using Eqs. (26) and (28) in Eq. (21):

$$\min_{(\pi,\omega,V)} H = -2\nu R V_{Tf}\cos\chi_{Tf}\cos\gamma_{Tf} \tag{30}$$

The normalized energy adjoint p_E and multiplier $\tilde{\mu}$ are now defined as

$$p_E = \frac{\lambda_E}{2\nu R} \tag{31}$$

$$\tilde{\mu} = \frac{\mu}{2\nu R} \tag{32}$$

respectively. Then Eq. (30) may be written as

$$\min_{(\pi,\omega,V)} \tilde{H} = -V_f\cos\chi_f \tag{33}$$

where, from Eqs. (21), (27), (31), and (32)

$$\tilde{H} = -V\cos\chi - y\omega f + p_E V(A\pi - B - C\omega^2) + \tilde{\mu}(V - V_m)(V - V_M) \tag{34}$$

The variation of $\tilde{H}$ with V is quite complex. Minimum $\tilde{H}$ is found through a numerical search. At each value of V, the extremal values of π and ω are found from Eqs. (33) and (34) as

$$p_E < 0: \quad \pi = 1, \qquad \omega = \text{sat}(-yf/2CVP_E) \tag{35}$$

$$p_E > 0: \quad \pi = 0, \qquad \omega = \text{sgn}(y) \tag{36}$$

where the normalized energy adjoint satisfies

$$\dot{p}_E = y\omega\partial f/\partial E + P_E V(\partial B/\partial E + \omega^2\partial C/\partial E - \pi\partial A/\partial E) + \tilde{\mu}[(V - V_M)\,\mathrm{d}V_m/\mathrm{d}E + (V - V_m)\,\mathrm{d}V_M/\mathrm{d}E] \tag{37}$$

It is seen that the throttle is switched at the zeros of p_E. For zero throttle, the bank angle is switched at the zeroes of y.

From Eq. (34), the variation of $\tilde{H}$ with V is composed of three terms, the typical variation of each of which is shown in Fig. 4. The first term, $-V\cos\chi$ is a line of constant slope. The $-y\omega f$ term decreases until a cusp is reached at the corner velocity V_c and then increases. The third term typically increases until V_c is reached, where there is a cusp owing to the $\tan\theta_M$ term in C. The curve then may descend through an inflection point because of the transonic drag rise, and then eventually begin to rise again. Combining these terms gives the typical variation in $\tilde{H}$ with V shown in Fig. 5. There are generally five possibilities for min H; at V_m, V_c, V_M, or at one of the two local minima V_{r1} and V_{r2}. At the local minima and on the speed bounds, additionally, $\partial H/\partial V = 0$, that is,

$$-p_E(B + C\omega^2 - A\pi) - p_E V\left(\frac{\partial B}{\partial V} + \frac{\partial C}{\partial V}\omega^2 - \frac{\partial A}{\partial V}\pi\right) - \cos\chi - y\frac{\partial f}{\partial V}\omega + \tilde{\mu}(2V - V_m - V_M) = 0 \tag{38}$$

On the speed bounds, Eq. (38) is used to compute $\tilde{\mu}$. At each point on the trajectory, a numerical search determines the values of $\tilde{H}$ at the corner velocity, at all local minima, and at the speed bounds. The value of the speed that gives the global minimum of $\tilde{H}$ is taken as the extremal speed.

Singular controls in throttle arise when p_E is zero over a finite time interval. This requires $\dot{p}_E \equiv 0$, giving from Eq. (37)

$$y\omega(\partial f/\partial E) + \tilde{\mu}[(V - V_M)\,\mathrm{d}V_m/\mathrm{d}E + (V - V_m)\,\mathrm{d}V_M/\mathrm{d}E] = 0 \tag{39}$$

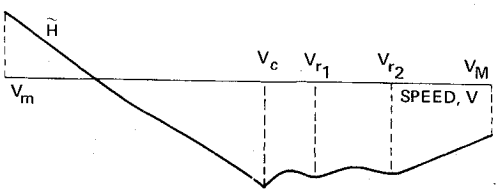

Fig. 5 A typical variation of $\tilde{H}$ with speed.

Equations (33) and (34) now simplify to

$$\min_{(\omega,V)} [-V\cos\chi - y\omega f + \tilde{\mu}(V - V_m)(V - V_M)] = -V_f\cos\chi_f \tag{40}$$

For a local minimum of $\tilde{H}$ with respect to speed occurring on the speed bounds, Eq. (38) holds, giving

$$-\cos\chi - y\omega\partial f/\partial V + \tilde{\mu}(2V - V_M - V_m) = 0 \tag{41}$$

From Eq. (40), the minimizing value of ω is

$$\omega = \text{sgn}(y) \tag{42}$$

unless $y \equiv 0$, in which case $\omega \equiv 0$. If the value of V minimizing Eq (40) is V_c, then Eq. (39) requires $y \equiv 0$ (at V_c, $\partial f/\partial E$ is nonzero). But then, if $y \equiv 0$ the minimizing value of V in Eq. (40) should be on a speed bound, a contradiction. For $V_c < V < V_M$, $\partial f/\partial E = 0$, but Eqs. (40) and (41) can be satisfied together only if

$$|y| = V_f\cos\chi_f/2f \tag{43}$$

at all points of the singular arc, which is unlikely. If $V = V_M$, $\partial f/\partial E = 0$ and Eqs. (39)-(41) require $\mathrm{d}V_M/\mathrm{d}E = 0$. Such singular arcs must remain on the maximum velocity limit where $\mathrm{d}V_M/\mathrm{d}E = 0$ (Fig. 1). Flight with a rectilinear projection in a horizontal plane, with the throttle set for constant energy satisfies Eqs. (39)-(41). With full bank, the energy will decrease with time, changing f and almost never in practice satisfying Eq. (41) over a finite time interval. As in the horizontal plane problem,[10] a bank-chattering arc is an extremal possibility.

Note that differential Eqs. (7) and (37), together with the extremal controls as obtained from Eq. (33), contain no refeence to the target motion; therefore, the same type of uncoupled open-loop optimality found in the horizontal plane analyses[6-11] is obtained here. Backward integration of the extremals depends only on the terminal-velocity vector of the interceptor and is independent of target motion. The characteristics of the extremal paths flown by the interceptor can be studied independently of the target motion. Specific encounters may then be obtained by combining the appropriate interceptor and target paths and checking for satisfaction of the capture criterion.

Each extremal is specified by the triplet $(E_f, \chi_f, \Delta\tau)$, the terminal energy, terminal heading, and trajectory time. Since the energy and heading adjoints vanish at termination, minimization of the Hamiltonian requires the interceptor's terminal speed to be

$$\left.\begin{aligned} V_f &= V_M, \quad \cos\chi_f > 0 \\ V_f &= V_m, \quad \cos\chi_f < 0 \end{aligned}\right\} \tag{44}$$

The terminal value of the multiplier $\tilde{\mu}$ is computed from Eq. (38) as

$$\tilde{\mu}_f = |\cos\chi_f|/(V_M - V_m) \tag{45}$$

Replacing y and p_E in Eqs. (35) and (36) by their corresponding time derivatives, the terminal throttle setting

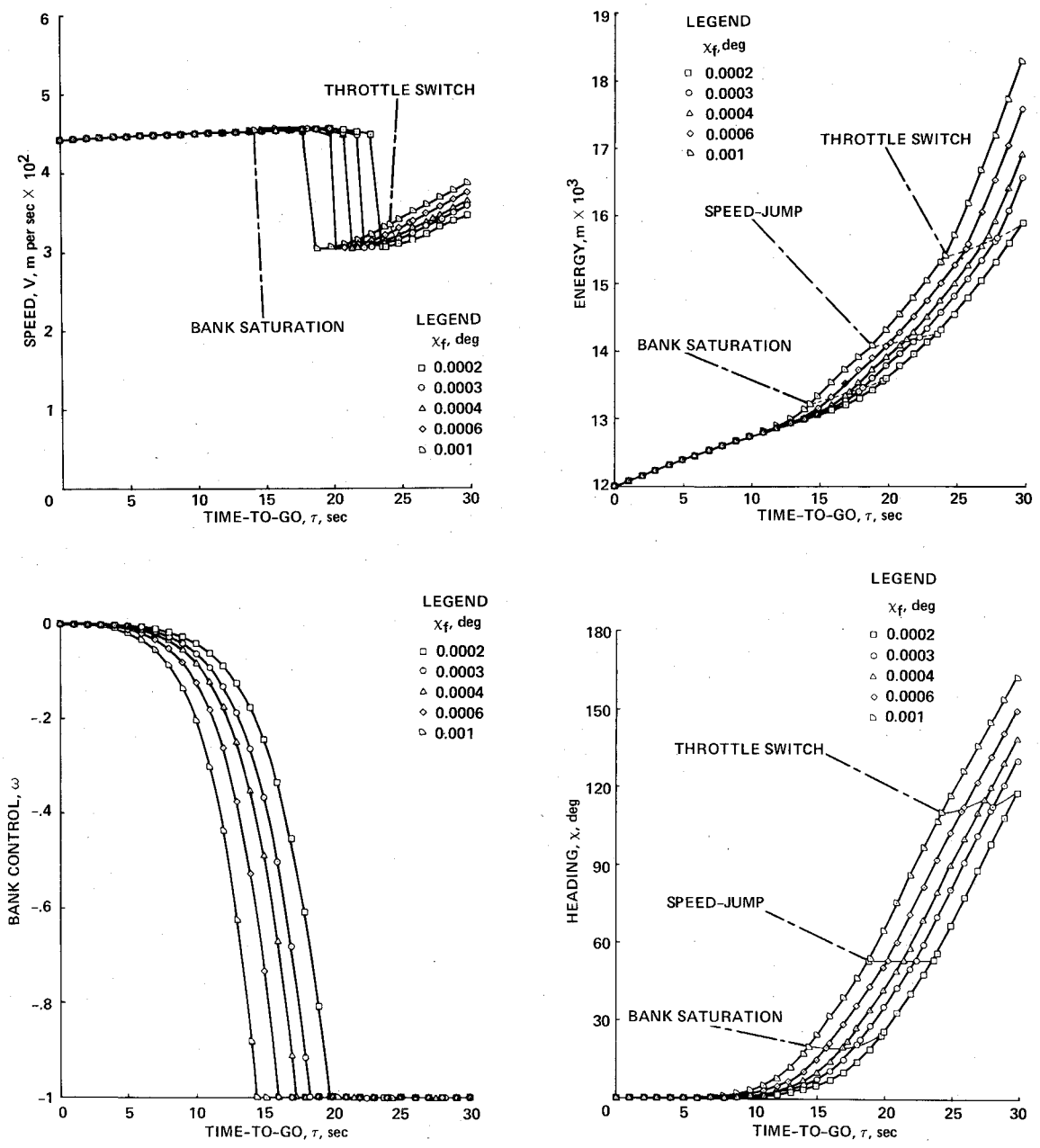

Fig. 6 Variations along extremals: final energy is 12,000 m; time marked at 1-s intervals and switch points. a) Speed variation. b) Bank variation. c) Energy variation. d) Heading variation.

and bank control values are given as follows; if $dV/dE \cos\chi_f > 0$ then

$$\left.\begin{aligned} \pi_f &= 1 \\ \omega_f &= -f\tan\chi_f/(2C\,dV/dE) \end{aligned}\right\} \tag{46}$$

and if $dV/dE\cos\chi_f > 0$, then

$$\left.\begin{aligned} \pi_f &= 0 \\ \omega_f &= -\mathrm{sgn}(\sin\chi_f) \end{aligned}\right\} \tag{47}$$

where $V = V_m$ or V_M.

If, for any τ, the speed at the global minimum is on a bound, $\bar{\mu}$, as computed from $\partial\tilde{H}/\partial V = 0$, must be positive. The matching of the two sides of Eq. (33) within a specified tolerance is used as an integration-error control. The step-size of the fourth-order Runge-Kutta routine is reduced when the per-step integration error exceeds an error bound. This is usually required in the vicinity of jumps in speed between local minima (see Fig. 5) and throttle switches.

Numerical Examples

Time histories of example extremal trajectories for two of the control variables (V and ω) and two of the state variables (E and χ) are shown in Fig. 6. The aircraft is the F4-C as modeled in Ref. 16. All trajectories are of 30-s duration, terminate with an energy of 12,000 m, but have different terminal headings. In forward time ($t = t_f - \tau$), the extremal values of V (Fig. 6a) start out on the corner velocity and then subsequently switch to the upper speed bound. In general, therefore, if the interceptor's speed is not equal to the corner velocity at the beginning of the trajectory and if its altitude is not within δh of the target's altitude at termination, the interceptor's speed time-history will consist of: 1) an initial jump to V_c, 2) a time interval spent at V_c, 3) an interior jump from V_c to V_M, 4) a time interval spent at V_M, and 5) a final jump to allow matching with the target's altitude at termination. The extremal values of ω (Fig. 6b) begin on the lower bound and then make the transition to near zero bank at termination. Thus, these extremal trajectories start with the controls set for MITR ($V = V_c$ and $\omega = -1$) and end with the

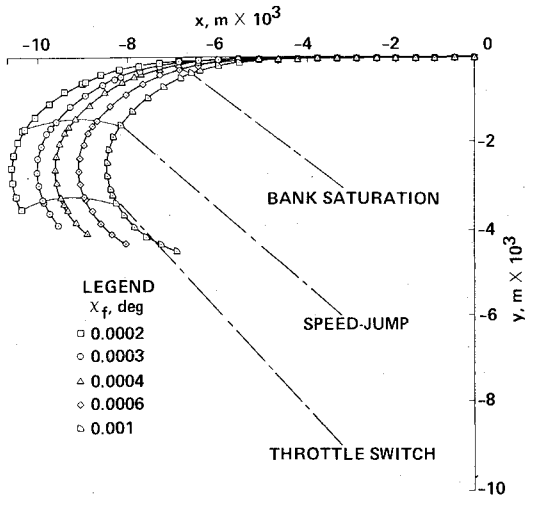

Fig. 7 Extremal trajectory projection on a horizontal plane: final energy is 12,000 m; final time is 30 s; time marked at 1-s intervals and switch points.

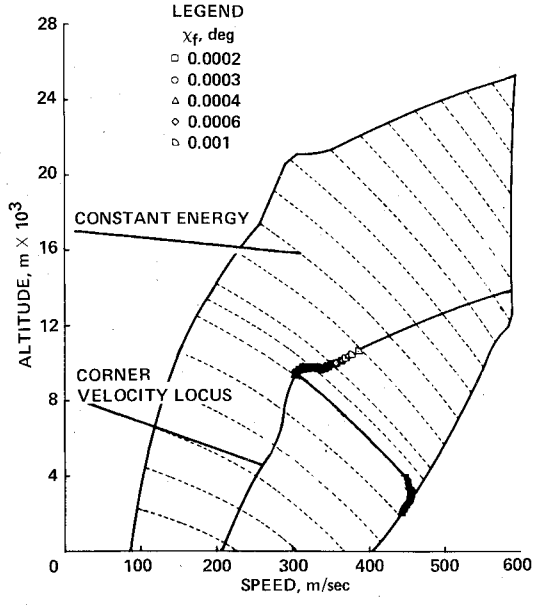

Fig. 8 Speed-altitude profile for extremals: final energy value = 12,000 m; final time = 30 s, time marked at 1-s intervals.

controls set for maximum speed ($V = V_M$ and $\omega \approx 0$). In all cases, the interior jump in V occurs before the bank saturates (in forward time). Some of the trajectories start with zero throttle ($\pi = 0$) and shortly switch to full throttle ($\pi = 1$), whereas the others have full throttle at all times. The energy-state variable (Fig. 6c) and heading-state variable (Fig. 6d) exhibit a steady decrease in forward time for all cases. The discontinuous changes in slope in E and χ are due to the jumps in V and π.

The paths of the extremal trajectories in the horizontal plane are shown in Fig. 7. Here the characteristic of hard turning followed by a high-speed dash is apparent. This characteristic results from the relatively large ratio of initial horizontal line-of-sight length to capture radius (r/R); for lower values of this ratio, extremal trajectories consisting of only hard turning may appear. The paths shown in Fig. 7 are very similar to the extremal paths of target interception in the horizontal plane.[6-11]

The extremal trajectories in the $h - V$ plane (Fig. 8) show once again that the paths start out on the corner-velocity locus. They then jump, at nearly the same value of energy for

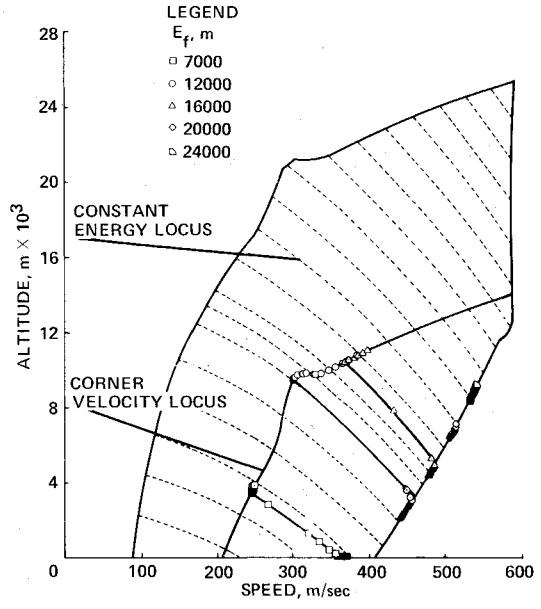

Fig. 9 Speed-altitude profile for extremals: final heading value = 0.001 deg; final time = 30 s, time marked at 1-s intervals.

all, to an interior minimum (V_{r2} of Fig. 5) and then, as V_{r2} approaches V_M, smoothly transit to the upper speed boundary.

In Fig. 9, the paths are shown for a family of extremal trajectories of fixed duration and final heading but with different values of final energy. The path with the highest final energy ($E_f = 24{,}000$ m) lies entirely on the maximum speed boundary. The path with $E_f = 20{,}000$ m is on this boundary except for a small portion with $V = V_{r2}$. Both these trajectories show very little change in speed, altitude, and heading. The $E_f = 16{,}000$ m and $E_f = 12{,}000$ m paths show the jump from V_c to V_{r2} and then the transition to V_M characteristic of the paths on Fig. 8. The $E_f = 7{,}000$ m path exhibits an additional feature. The trajectory starts in forward time on the corner-velocity locus, but then the relative local minimum V_{r1} of Fig. 5 appears at V_c, moves to the right, and, for a time, gives a global minimum of $\tilde{H}$. The speed control then jumps to V_{r2}, finally making the transition to V_M. Note that for $E_f = 7{,}000$ m the trajectory ends with speed increasing, whereas for all other trajectories speed is decreasing at termination.

Concluding Remarks

Three-dimensional extremal trajectories for minimum-time target interception have been obtained by using an energy-state dynamic model and realistic aerodynamic- and propulsive-force models for a high-performance aircraft (F4-C). The extremal paths generally begin on the corner-velocity locus and then jump to the maximum speed boundary, although short periods of local relative extremal control often appear as well.

For implementation in an on-board flightpath management system, the open-loop results of the present paper must be put in feedback form. This can be accomplished in the same manner as has been done for target interception in a horizontal plane. However, this still leaves the question of the large jumps in speed, a consequence of the energy-state modeling. This can be accounted for by using the boundary-layer methods of singular-perturbation theory.

References

[1] Well, K.H., Faber, B., and Berger, E., "Optimization of Tactical Aircraft Maneuvers Utilizing High Angles of Attack," *Journal of Guidance and Control*, Vol. 5, March-April 1982, pp. 131-137.

[2]Jarmark, B.S.A., Merz, A.W., and Breakwell, J.V., "The Variable-Speed Tail-Chase Aerial Combat Problem," *Journal of Guidance and Control,* Vol. 4, May-June 1981, pp. 323-328.

[3]Ardema, M.D. and Rajan, N., "Separation of Time-Scales in Aircraft Trajectory Optimization," AIAA Paper 83-2136, 1983.

[4]Shinar, J., Farber, N., and Negrin, M., "A Three-Dimensional Air Combat Game Analysis by Forced Singular Perturbations," AIAA Paper 82-1327, 1982.

[5]Calise, A.J., "Singular Perturbation Techniques for On-Line Optimal Flight Path Control," *Journal of Guidance and Control,* Vol. 4, July-Aug. 1981, pp. 398-405.

[6]Rajan, N., Prasad, U.R., and Rao, N.J., "Pursuit-Evasion of Two Aircraft in a Horizontal Plane," *Journal of Guidance and Control,* Vol. 3, May-June 1980, pp. 261-267.

[7]Prasad, U.R., Rajan, N., and Rao, N.J., "Planar Pursuit-Evasion with Variable Speeds, Part 1, Extremal Trajectory Maps," *Journal of Optimization Theory and Applications,* Vol. 33, No. 3, March 1981, pp. 401-418.

[8]Rajan, N., Prasad, U.R., and Rao, N.J., "Planar Pursuit-Evasion with Variable Speeds, Part 2, Barrier Sections," *Journal of Optimization Theory and Applications,* Vol. 33, No. 3, March 1981, pp. 419-432.

[9]Rajan, N. and Prasad, U.R., "The Extremal Trajectory Map: A New Representation of Combat Capability," AIAA Paper 79-1622, Boulder, Colo., 1979.

[10]Rajan, N. and Ardema, M.D., "Barriers and Dispersal Surfaces in Minimum-Time Interception," NASA TM-84241, 1982.

[11]Rajan, N. and Ardema, M.D., "Computations of Optimal Feedback Strategies for Interception in a Horizontal Plane," AIAA Paper 83-0281, 1983.

[12]Kelley, H.J., "Aircraft Maneuver Optimization by Reduced Order Approximations," *Advances in Control and Dynamic Systems,* Vol. 10, Academic Press, New York, 1973, pp. 131-178.

[13]Ardema, M.D., "An Introduction to Singular Perturbations in Nonlinear Optimal Control," *Singular Perturbations in Systems and Control,* M.D. Ardema, ed., Courses and Lectures No. 280 International Center for Mechanical Sciences, Udine, Italy, 1983, pp. 1-92.

[14]Bryson, A.E., Jr. and Ho., Yu-Chi, *Applied Optimal Control,* Blaisdell, Waltham, Mass., 1969, pp. 108-109.

[15]Leitmann, G., *An Introduction to Optimal Control,* McGraw-Hill Book Co., New York, 1966, pp. 25-26.

[16]Parsons, M.G., "Three-Dimensional, Minimum Time Turns to a Point and onto a Line for a Supersonic Aircraft with a Constraint on Maximum Velocity," Ph.D. Dissertation, Stanford University, Stanford, Calif., 1972.